


RESEARCH

Open Access



# Alkali-Silica Reaction and Residual Mechanical Properties of High-Strength Mortar Containing Waste Glass Fine Aggregate and Supplementary Cementitious Materials

Hamin Eu<sup>1</sup>, Gyuyong Kim<sup>1\*</sup> , Minjae Son<sup>2</sup>, Sasui Sasui<sup>1</sup>, Yaechan Lee<sup>1</sup>, Hyeonggil Choi<sup>3</sup>, Sukpyo Kang<sup>4</sup> and Jeongsoo Nam<sup>1</sup>

## Abstract

This paper presents the influence of supplementary cementitious materials (SCMs), such as fly ash (FA), silica fume (SF), ground granulated blast furnace slag (GGBS), and waste glass fine aggregate (GA), on the alkali-silica reaction (ASR) in high-strength and normal-strength mortar using an accelerated mortar bar test (AMBT). Residual mechanical properties and scanning electron micrographs were used to assess the changes in the matrix. GA reduced the mechanical properties of both normal-strength (NGA\_OPC) and high-strength mortars (HGA\_OPC), contributing to a decline in overall performance. This phenomenon was a result of the slipping of the GA from the matrix owing to its smooth surface. However, the inclusion of reactive SF and GGBS in the HGA improved the slip phenomenon of the GA, leading to a significant enhancement in its mechanical properties. Following the ASR expansion measurement, HGA\_OPC demonstrated an ASR expansion rate approximately three times higher than that of NGA\_OPC. This was attributed to the dense structure of HGA\_OPC, which resulted in greater expansion than that of NGA\_OPC. However, with the incorporation of SCMs into both HGA and NGA, a significant reduction in ASR expansion was observed. This was attributed to the delayed ASR of GA due to alkali activation or the pozzolanic reaction of the SCMs. Continuous exposure to the AMBT environment can lead to the destruction of GA. This was caused by the inner ASR that originated from the surface crack of the GA, which resulted in a reduction in the flexural strength of the mortar. The HGA with SF exhibited the highest resistance to ASR expansion and residual mechanical properties' degradation. Therefore, various durability and long-term performance-monitoring studies on ultra-high-performance concrete or high-strength cementitious composites with very high SF contents and GA can be conducted.

**Keywords** Waste glass fine aggregate, Mechanical properties, Alkali-silica reaction, Supplementary cementitious materials

Journal information: ISSN 1976-0485 / eISSN 2234-1315.

\*Correspondence:

Gyuyong Kim  
gyuyongkim@cnu.ac.kr

Full list of author information is available at the end of the article



© The Author(s) 2024. **Open Access** This article is licensed under a Creative Commons Attribution 4.0 International License, which permits use, sharing, adaptation, distribution and reproduction in any medium or format, as long as you give appropriate credit to the original author(s) and the source, provide a link to the Creative Commons licence, and indicate if changes were made. The images or other third party material in this article are included in the article's Creative Commons licence, unless indicated otherwise in a credit line to the material. If material is not included in the article's Creative Commons licence and your intended use is not permitted by statutory regulation or exceeds the permitted use, you will need to obtain permission directly from the copyright holder. To view a copy of this licence, visit <http://creativecommons.org/licenses/by/4.0/>.

## 1 Introduction

Natural sand from seas and rivers has traditionally been used as a fine aggregate for concrete and mortar in the construction industry. However, because of the destruction of natural ecosystems and limited resources, studies have been conducted on the development of recycled aggregates (Kwan et al., 2012; Padmini et al., 2009; Sasui et al., 2023; Tabsh & Abdelfatah, 2009). Additionally, many countries, including Hong Kong, the United States, Japan, and Europe, face environmental issues caused by the indiscriminate discharge of soda-lime glass bottles and a lack of landfills. In the case of glass bottles, only approximately 60–70% are currently recycled, and the rest end up in landfills, because recycling becomes challenging when their colors are not distinguished or when they are broken. Therefore, various studies have been conducted, and policies have been established regarding the treatment of waste glass bottles. Since the 1990s, numerous researchers have conducted studies on recycling waste glass bottles as construction materials, including powders and aggregates (Ahmad et al., 2022; Omran et al., 2017; Sasui et al., 2020, 2021, 2022; Shayan & Xu, 2004, 2006; Shi et al., 2005; Taha & Nounu, 2009; Tittarelli et al., 2018). Waste glass can be utilized as an aggregate owing to its similar density to that of conventional aggregates and nearly zero water absorption rate.

However, many researchers have reported that the use of waste glass fine aggregate (GA) in mortar and concrete degrades its mechanical properties and causes an alkali-silica reaction (ASR). The smooth surface and sharp grain shape of GA reduce its bond strength with the cement matrix, thereby degrading its mechanical properties. Tan and Du (2013) reported the compressive strength of glass aggregate (GA) mortar. The compressive strength of GA mortar can be decreased by the sharp grain shape and smooth surface of the GA, leading to weaker bonding between the cement matrix and GA in the interfacial transition zone (ITZ) (Kou & Poon, 2009). In addition, GA is known to generate expansion cracks in the cement matrix by reacting with the highly alkaline cement and causing ASR owing to its composition of amorphous silica (Park & Lee, 2004; Rashad, 2014; Tan & Du, 2013). Therefore, previous studies have suggested the use of supplementary cementitious materials (SCMs) or a reduction in the amount of GA (Du & Tan, 2013; Lu et al., 2017). Lu et al. evaluated the compressive and flexural strengths of white cement mortar containing 100% GA and SCMs [fly ash (FA), ground granulated blast furnace slag (GGBS), Metakaolin (MK), and glass powder]. They reported that SCMs could improve the strength of mortar if used appropriately. This is owing to the possible filling effect of the small particles and the granular shape of the SCMs (Lu et al., 2017). Du and Tan

studied the ASR of GA mortar specimens mixed with FA (30%) instead of cement and reported that FA inhibited the ASR of GA (Du & Tan, 2013). ASR expansion and cracking were not observed in the FA-mixed GA mortar specimens. FA can control the ASR by reducing the alkali content and porosity of the cement matrix via a pozzolanic reaction. Furthermore, the ASR expansion of glass sand mortars replacing 60% of cement with GGBS, was evaluated. They reported that GGBS, similar to FA, reduced the ASR expansion of FA mortar. In the case of silica fume (SF), the ASR of GA mortar was confirmed to be effectively controlled when 10% of cement was replaced with SF (Du & Tan, 2013; Duchesne and Bérubé 1994a, b; Xu et al., 1995).

Recently, many studies have been conducted to apply GA to high-strength concrete or UHPC where various SCMs are used together. Soliman and Tagnit-Hamou investigated the performance of UHPC with GA instead of quartz sand (QS) (Soliman & Tagnit-Hamou, 2017). They reported that GA with a particle size of 275  $\mu\text{m}$  can replace the QS of UHPC. Although the mechanical properties of UHPC are reduced, it has not occurred harmful ASR expansion. In addition, Y. Jiao et al. evaluated the mechanical properties by incorporating GA into UHPC (Jiao et al., 2020). As a result, when 75% of QS was replaced by GA, it was reported that the mechanical properties of UHPC increased. However, when 100% was replaced, the mechanical properties of UHPC decreased slightly. They reported that GA could be used for UHPC. Meanwhile, existing studies applying GA to high-strength cement composite such as UHPC mainly use the small particle size of GA. Many studies have reported that small particle size GA does not occur harmful ASR expansion (Corinaldesi et al., 2005; Rashad, 2014). However, making GA into powder and sand with small particle size consumes a lot of crushing energy. If GA with fine aggregate particle size, which consumes relatively little crushing energy, is used, the recycling rate of GA can be further increased. When incorporating GA with large particle size into high-strength concrete, the utilization of GA can be further increased if mechanical properties' degradation and harmful ASR expansion can be improved. Therefore, research is needed to use GA with large particle size, not small particle size, for high-strength mortar or concrete.

Additionally, ASR expansion degrades the mechanical properties of concrete by generating severe cracks in the cement matrix and on the surface. Therefore, the residual mechanical properties under ASR conditions must be evaluated. In this regard, some researchers have investigated the influence of ASR in concrete using reactive aggregates (amorphous silica, such as opal, chalcedony, cristobalite, and volcanic glass) on the residual

mechanical properties (Larive et al., 1996; Giaccio et al., 2008; Hajighasemali et al., 2014; Jones & Clark, 1996; Koyanagi et al., 1986; Siemes & Visser, 2000; Takemura et al., 1996). Previous studies have reported that the ASR gel expands by absorbing moisture, leading to a decrease in the elastic modulus and tensile strength of mortar and concrete (Jones & Clark, 1996; Siemes & Visser, 2000; Takemura et al., 1996). It is necessary to evaluate the residual mechanical properties by ASR in high-strength concrete incorporated with GA. In addition, various SCMs are used for high-strength concrete. These SCMs can affect the mechanical properties, ASR expansion behavior, and residual mechanical properties of GA high-strength concrete. However, studies on the residual mechanical properties of ASR in GA high-strength concrete using SCMs are insufficient.

Therefore, this study evaluated the mechanical properties and ASR expansion of high-strength mortars incorporating SCMs and GA. In addition, the residual mechanical properties due to the ASR expansion were assessed. The ASR expansion was assessed using the accelerated mortar bar method (AMBT), and for comparison with high-strength mortar, the same experiments were conducted using normal-strength GA mortar. Furthermore, an analysis of the correlation between the ASR expansion rate and residual mechanical properties was performed to understand the impact of ASR expansion on the mechanical properties of GA mortar. Thus, the feasibility of using GA in high-strength mortars and deriving appropriate SCMs is discussed.

## 2 Materials and Methods

### 2.1 Materials

Ordinary Portland cement (OPC), FA, SF, and GGBS as binders were used in this study. The chemical compositions of the binders used in this study were determined using X-ray fluorescence spectroscopy (XRF, ZSX Primus II, Rigaku) and are presented in Table 1. The FA used in this study is of the Class F type, sourced from Maxcon Co. Ltd., Korea. It mainly consists of SiO<sub>2</sub> and Al<sub>2</sub>O<sub>3</sub> and

has a density of 2.24 g/cm<sup>3</sup> and specific surface area of 3940 cm<sup>2</sup>/g. SF (Grade 940-U, Elkem Microsilica from ACS Co. Ltd., Korea) consists of more than 97% amorphous silica. It has a bulk density of 0.2–0.35 g/cm<sup>3</sup> and a specific surface area of 150,000–300,000 cm<sup>2</sup>/g. The GGBS (Maxcon Co., Ltd., Korea) is mainly composed of SiO<sub>2</sub>, Al<sub>2</sub>O<sub>3</sub>, and CaO and has a density of 2.90 g/cm<sup>3</sup> and specific surface area of 4580 cm<sup>2</sup>/g.

Natural fine aggregates (NA) and GA were used as fine aggregates. The GA used a mixture of three different types of glass cullets, each type with a different color. The company 'Indong G.R.C.' in the Republic of Korea supplied the glass cullet (2–5 mm) in three colors: transparent, green, and brown. These cullets were crushed using a ball mill in the laboratory to achieve a standard fine aggregate particle size. The crushed fine aggregates from the three colored glasses were mixed in the same ratio. Figs. 1 and 2 show the particle-size distribution curves and appearance of the NA and GA used, respectively. Both NA and GA satisfied the standard particle-size distribution of fine aggregates according to ASTM C33 (ASTM C33/C33M-18, 2010). On the other hand, according to ASTM C 1260, the particle-size distribution of fine aggregate used in ASR expansion rate test is specified. However, in this study, the standard particle size of existing fine aggregate was used, because the ASR expansion amount was compared relatively, not to check whether the aggregate expanded ASR or not. As shown in Fig. 2, the GA exhibited a smooth surface and a long, flat shape. Table 2 lists the physical properties and chemical compositions of the NA and GA used in this study. The chemical composition was also measured using XRF equipment. In the case of GA, the density was relatively low compared

**Table 1** Chemical composition of OPC and SCMs used

Chemical composition (wt%)	OPC	FA	SF	GGBS
SiO <sub>2</sub>	16.14	53.44	97.4	31.91
Al <sub>2</sub> O <sub>3</sub>	4.39	24.65	0.4	14.09
Fe <sub>2</sub> O <sub>3</sub>	3.83	7.49	0.1	0.79
CaO	66.79	3.87	0.2	46.44
MgO	2.47	0.58	0.6	2.53
K <sub>2</sub> O	1.19	1.38	0.9	0.49
Na <sub>2</sub> O	0.08	0.54	0.3	0.17

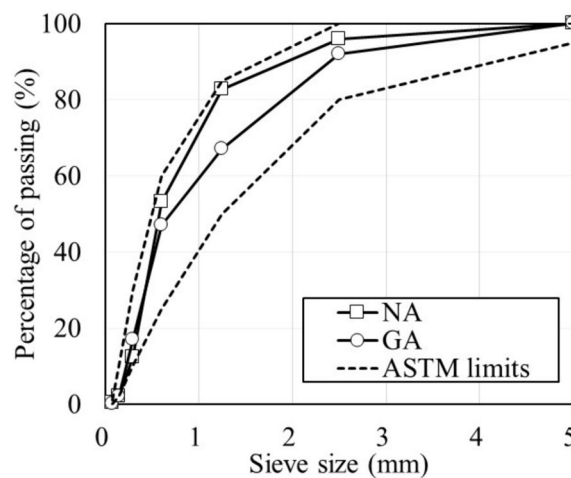


**Fig. 1** Particle-size distribution of NA and GA

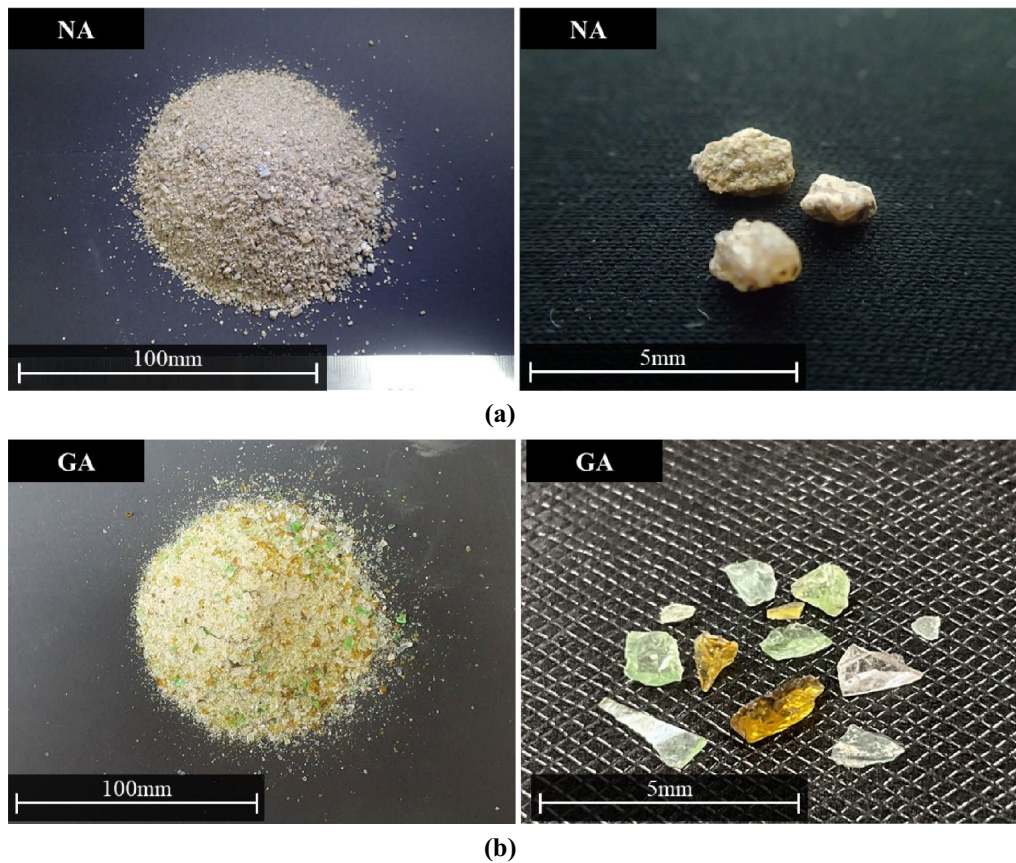


**Fig. 2** Appearance of NA and GA

**Table 2** Physical properties and chemical composition of NA and GA

Properties	NA	GA
Density (g/cm <sup>3</sup> )	2.54	2.45
Fineness modulus	2.53	2.95
Water absorption (%)	1.6	0.4
Chemical composition (%)		
SiO <sub>2</sub>	82.21	65.91
Al <sub>2</sub> O <sub>3</sub>	9.12	3.93
CaO	2.41	12.95
MgO	0.83	1.42
Na <sub>2</sub> O	1.91	10.23
K <sub>2</sub> O	1.62	0.98
Cr <sub>2</sub> O <sub>3</sub>	0.32	0.12
Fe <sub>2</sub> O <sub>3</sub>	2.15	0.43

with that of NA, but the water absorption was close to zero. The GA used in this study is made up of soda-lime glass bottles; therefore, most of the silica is amorphous. This has been widely reported in the previous studies; therefore, X-ray diffraction (XRD) analysis was not

conducted separately. GA showed a higher ratio of CaO and Na<sub>2</sub>O than NA.

### 2.2 Mix Proportion and Plan

Table 3 lists the mixing proportions of GA mortars. The IDs of the specimens were defined by the strength category (high or normal), aggregate type, and SCM. For instance, if the strength is normal, abbreviation ‘N’ is used, and if the strength is high, abbreviations ‘H’ is used. When the mortar consisted of GA without SCMs, the sample IDs NGA\_OPC for normal strength and HGA\_OPC for high strength were used. Similarly, the GA mortar with SCMs used the IDs NGA\_SCM or HGA\_SCM, where SCM stood for FA, SF, or GGBS.

For the normal-strength GA mortar, w/b was set to 0.5, and the fine aggregate-to-binder ratio (a/b) was set to 3, in accordance with ISO 679 (Cement-Test Methods-Determination of Strength, 2009). For the ASTM C 1260 samples, mixing ratios w/b=0.47 and a/b=2.25 were used (ASTM C1260-22, 2014). The replacement ratio of each SCM was as follows: FA: 20 wt.% of OPC; SF: 10 wt.% of OPC; GGBS: 40 wt.% of OPC. The replacement rate was determined by referencing previous studies on

**Table 3** Mix proportions and specimens IDs

Specimen ID. <sup>a)</sup>	Mix proportion (kg/m <sup>3</sup> )						SP (wt%) <sup>b)</sup>	
	Water	Binder				Fine aggregate		
		OPC	FA	SF	GGBS	NA		GA
NNA	256	512				1536		
NGA_OPC							1536	
NGA_FA		409.6	102.4				1536	
NGA_SF		460.8		51.2			1536	
NGA_GGBS		307.2			204.8		1536	
HNA	184	922				1383	1.7	
HGA_OPC							1383	
HGA_FA		737.6	184.4				1383	
HGA_SF		829.8		92.2			1383	
HGA_GGBS		553.2			368.8		1383	

<sup>a)</sup> N Normal-strength mortar (w/b: 0.5 and a/b: 3), H High-strength mortar (w/b: 0.2 and a/b: 1.5),

NA Natural fine aggregate, GA Waste glass fine aggregate

<sup>b)</sup> The percent of addition amount by weight of binder

the incorporation amounts of SCMs aimed at reducing initial compressive strength loss due to excessive incorporation and mitigating the ASR of GA (Du & Tan, 2013; Lu et al., 2017). To maximize the effect of GA incorporation, 100% GA was used.

For the high-strength GA mortar, w/b was set to 0.2 and a/b was set to 1.5. To secure a slump due to the low w/b of the high-strength mortar, a/b was set to 1.5. Because the mixing ratio for the high-strength mortar for ASR expansion was not specified, the same ratio (w/b=0.2 and a/b=1.5) was used for ASR expansion specimen. The replacement rate for each SCM was the same as that for the normal GA mortar. Because the w/b ratio of the high-strength GA mortar was very low, polycarboxylate superplasticizer (SP) (Flowmix 3000S, Dongnam Co., Korea) was used to improve the slurry workability. Its content was 1.7% of the binder weight for HNA and HGA. However, for high-strength GA mortars with SCMs, the content of SP was 1.275% to control the slump, which may have increased owing to the water demand reduction effect of SCMs. The SP used in this study was chloride-free and had a low alkali content.

The binders and fine aggregate were mixed using a mortar mixer, and dry mixing was performed for approximately 60 s. Water was then added, and mixing was performed for approximately 120 s. For the high-strength mortar, the superplasticizer was slowly added, and further mixing was performed for 60–120 s. After pouring into the mold, vibratory compaction was performed for approximately 30 s using a shaking table. For the high-strength mortar, vibratory compaction was performed for 15 s when SP was used to prevent bleeding. The

mortar specimen was cast in a mold and cured in the air at 25 ± 2 °C and a relative humidity (RH) of 60 ± 5% for 1 day. The exposed surface of the mortar was covered with vinyl to minimize moisture evaporation. After demolding, the mortar specimen was cured in water at 25 ± 2 °C.

### 2.3 Test Method

#### 2.3.1 Flow and Air Content

The flow was derived from the average diameter of the mortar after pouring the mortar into a cone installed on the mortar flow table and striking the flow Table 25 times in accordance with ASTM C1437 (ASTM C, 1293 2015). The air content was evaluated immediately after mortar mixing using air content equipment in accordance with EN 1015–7 (“EN 1015-7: 2007. Methods of test for mortar masonry—part 7: determination of air content of fresh mortar.” n.d.). The measurement time did not exceed five minutes for any specimen.

#### 2.3.2 Mechanical Properties

To measure the compressive and flexural strengths, 40 mm × 40 mm × 160 mm specimens were prepared in accordance with ISO 679. They were poured into the mold and subjected to air-dry curing under 25 °C and 60% RH conditions for 24 h. They were then removed from the mold and subjected to water curing at 20 °C. The specimens were removed from the water after 7, 28, 56, and 91 days of water curing to measure their strength. A three-point flexural strength test was conducted at a loading rate of 50 N/s, and the compressive strength was measured at a loading rate of 2,400 N/s until the specimen fractured. The maximum strength was measured

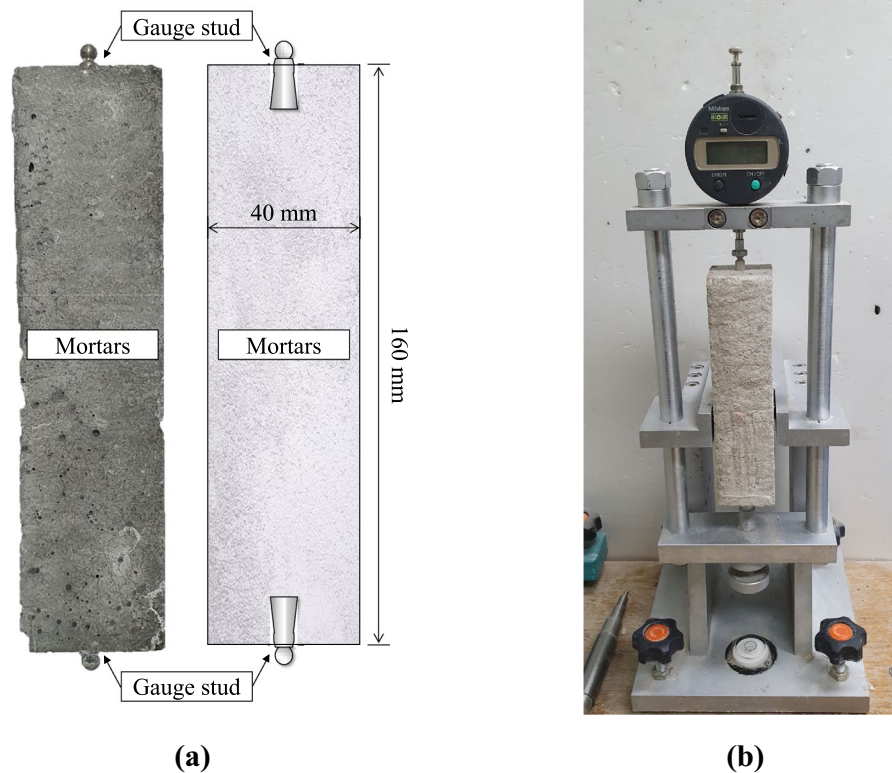


**Fig. 3** Mortar and length change-measuring instrument used for measuring the residual mechanical properties after AMBT. **a** Mortars specimens and gauge stud. **b** Length change-measuring instrument

(Cement-Test Methods-Determination of Strength, 2009).

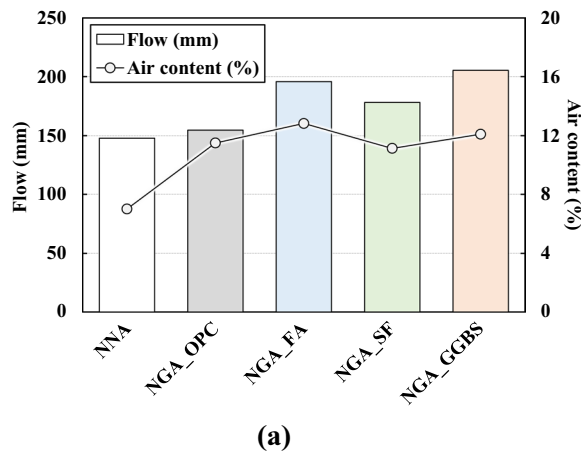
### 2.3.3 ASR Expansion Rate (Accelerated Mortar Bar Method, AMBT)

The ASR expansion rates of the normal and high-strength GA mortars mixed with SCMs were evaluated according to ASTM C1260 and C1567 (AMBT) (ASTM C1567-04 2005). The specimens had dimensions of 25 mm × 25 mm × 285 mm. The change in length according to the ASR expansion was measured by inserting gauge studs at both ends of the mortar specimen, in accordance with ASTM C490 (ASTM C490, 2017; ASTM C1260-22, 2014). The prepared ASR specimens were cured in water at 80 °C for 24 h, and the length of each specimen before the accelerated ASR was measured. The specimens were then immersed in a 1 N NaOH solution at 80 °C. They were removed from the solution at regular intervals to measure the changes in length. The expansion rate was derived by comparing the measured specimen length with its length before immersion in the solution. Three samples were tested for each type, and the average values were used. Measurements were performed

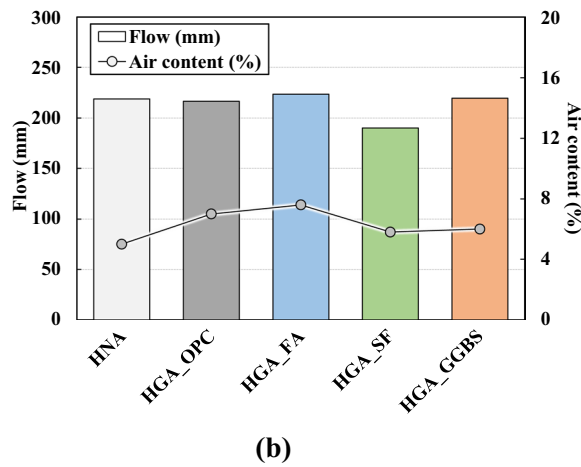
daily for 28 days. Meanwhile, NA and GA of fine aggregate standard particle size were used in this experiment. Also, there is no standard for measuring the ASR expansion of reactive aggregates in high-strength mortars, the ASR expansion rate was evaluated using the same AMBT. Although the presented expansion criterion (0.1% on the 14th day) could not be directly and equally applied, the relative amounts of expansion were compared instead.

### 2.3.4 Residual Mechanical Properties Under AMBT

Considering that ASR is a slow reaction, a considerable amount of time is required to evaluate the degradation of mechanical properties caused by it. Therefore, in this study, the residual mechanical properties were evaluated after the ASR accelerating condition using the AMBT method (Du & Tan, 2013; Mohammadi et al., 2020). The residual mechanical properties after AMBT were evaluated at 3, 7, and 28 days. For each evaluation, the specimen's surface was wiped, followed by drying at a constant temperature and humidity (25 °C and 60% RH) for approximately 3 h. The change in the length of the mortar was measured immediately before evaluating the residual compressive and flexural strengths. Similar specimens to

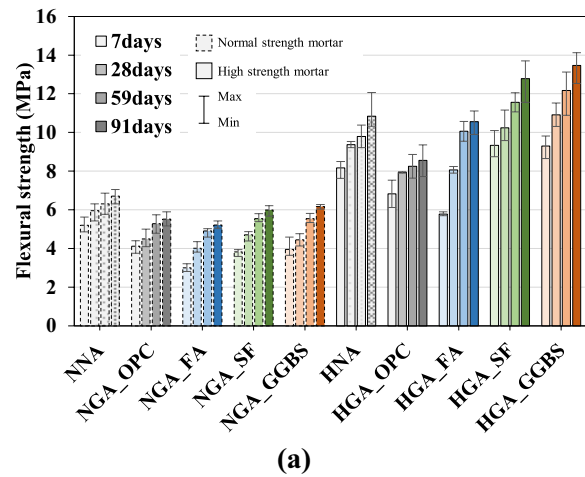


(a)

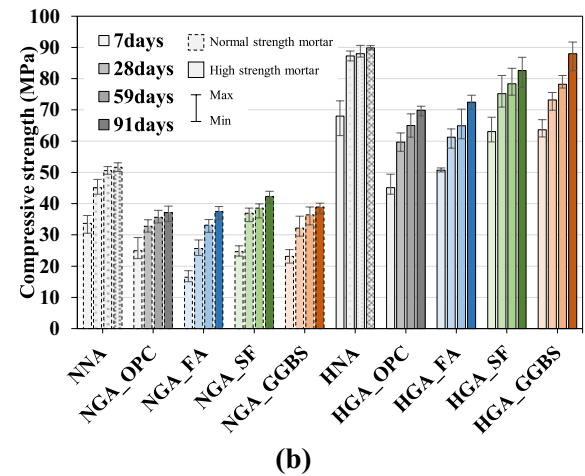


(b)

**Fig. 4** Results of flow and air content. **a** NGA mortar groups. **b** HGA mortar groups



(a)



(b)

**Fig. 5** Mechanical properties of GA mortar according to age. **a** Flexural strength. **b** Compressive strength

those used in the mechanical property test described in Sect. 2.3.2 were prepared. Gauge studs were embedded at both ends of each specimen to measure the change in length (see Fig. 3a). The initial lengths of all specimens before immersion in the solution were measured using a length change-measuring instrument (see Fig. 3b).

**2.3.5 Microstructure Analysis**

After the AMBT, a microstructure analysis was conducted to confirm the microstructure and conditions of the GA. Mortar specimens were collected and immediately immersed in ethanol for 1 day. Subsequently, the specimen was immediately cut using a diamond saw and impregnated with epoxy. Then, grinding was performed using SiC, and polishing was performed using diamond and colloidal silica. The microstructure was analyzed using scanning electron microscopy (SEM; Merlin Compact, Carl Zeiss, Germany). Microstructural images were captured in the backscatter detector mode (SEM-BSE).

**3 Experimental Results and Discussions**

**3.1 Flow and Air Content**

Fig. 4 shows the flow and air content of normal and high-strength GA mortars with added SCMs. As shown in Fig. 4a, NGA\_OPC exhibited a higher air content than NNA. This is attributed to the low water absorption rate of GA and its long, flat particle shape (Drzymala et al., 2020). This increase in air content was expected to have a negative impact on the mechanical properties of the mortar. When SCMs were added, the flow significantly increased compared with NNA and NGA\_OPC, owing to the workability improvement effect. FA can improve the coefficient of friction between cement particles owing to its round shape, thereby increasing the flow (Du et al., 2021). However, SF has been shown to have relatively small flows compared to FA and GGBS, owing to its very high fineness. SF is known to make mortar sticky. The highest slump was observed for GGBS. This appears to be due to the smooth, glassy surface. In the case of the

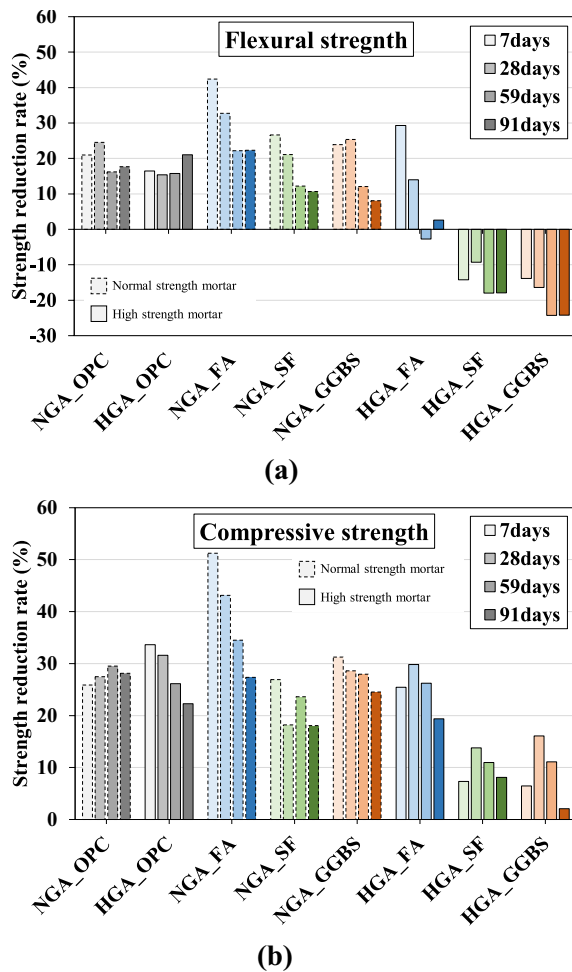


**Fig. 6** Strength reduction rate of GA mortar according to age. **a** Flexural strength. **b** Compressive strength

high-strength mortar, as shown in Fig. 4b, the slump was very high owing to the use of SP. The slumps of the HNA and HGA\_OPC exhibited similar values. For HGA\_SF, however, the flow significantly decreased owing to the microparticles and high fineness, as in the case of the normal-strength GA mortar, despite the use of SP. The amount of air showed a tendency similar to that of the normal-strength GA mortar.

### 3.2 Mechanical Properties

Fig. 5 shows the flexural and compressive strengths of the GA mortars mixed according to age. NGA\_OPC and HGA\_OPC have reduced flexural and compressive strengths compared to the NNA and HNA mortars, regardless of age. This is believed to be due to the reduced adhesion to the cement matrix owing to the smooth surface of the GA (Drzymala et al., 2020). This decrease in adhesion can cause a slip in the GA. The slip of the GA

did not share the stress and was easily separated from the cement matrix when the mortar was broken. Accordingly, the slip of GA can degrade its mechanical properties (Du & Tan, 2017; Hamada et al., 2022). Meanwhile, a high-strength cement matrix may increase the bond strength between the GA and cement matrix. However, the strength of HGA\_OPC was reduced by up to about 34% compared to HNA. The strength of NGA\_OPC was reduced by up to about 20% compared to NNA. Yin et al. (2023) evaluated the mechanical properties of high-strength cement (HPC) materials with a water/binder ratio of 0.2 with 20% GA content. They also reported that the reduction rates of compressive and flexural strengths of HPC were 10.7% and 9.1%, respectively. They also reported this phenomenon as a reason for the weakening of the bond strength due to the smooth surface of GA. In this study, it was also found that HGA\_OPC did not improve the slip of GA.

The results of GA mortar incorporating SCMs are as follows. The NGA\_SCMs exhibited lower flexural and compressive strengths than the NGA\_OPC. This was due to the cement dilution effect caused by the mixing of SCMs. However, the HGA\_SCMs exhibited a significant increase in flexural and compressive strengths compared to the HGA\_OPC. In particular, mixing SF and GGBS significantly improved the flexural strength. The flexural strengths of HGA\_SF and HGA\_GGBS exceeded the strength of HNA with increasing age. Because SF has a very small particle size (0.1–0.3 μm) and high reactivity, it can improve the cement matrix of high-strength mortar with the filling effect and pozzolanic reaction. In the case of GGBS, previous studies have reported that the shape of the GGBS particles is long and elongated, which can further increase the flexural strength (Lu et al., 2017).

Fig. 6 shows the strength reduction rate of the specimens at each age, with the NGA groups representing the NNA and the HGA groups representing the HNA. Despite the high-strength cement matrix of the HGA\_OPC, its strength decreased to a level similar to that of the NGA\_OPC. However, the addition of SCMs to HGA had a more pronounced effect on improving its mechanical properties than their addition to NGA. In particular, when SF and GGBS were mixed, the flexural strength improved significantly. This is believed to be due to the fact that the pore filling effect by the pozzolanic reaction of SCMs was better exhibited in the high-strength mortar with a dense structure than in the normal-strength mortar. To confirm this, the fracture cross-section of the mortar test was investigated.

Fig. 7 shows the fractured cross-section after the flexural strength test of the high-strength mortar to check the slip of the GA. The HNA showed that all the



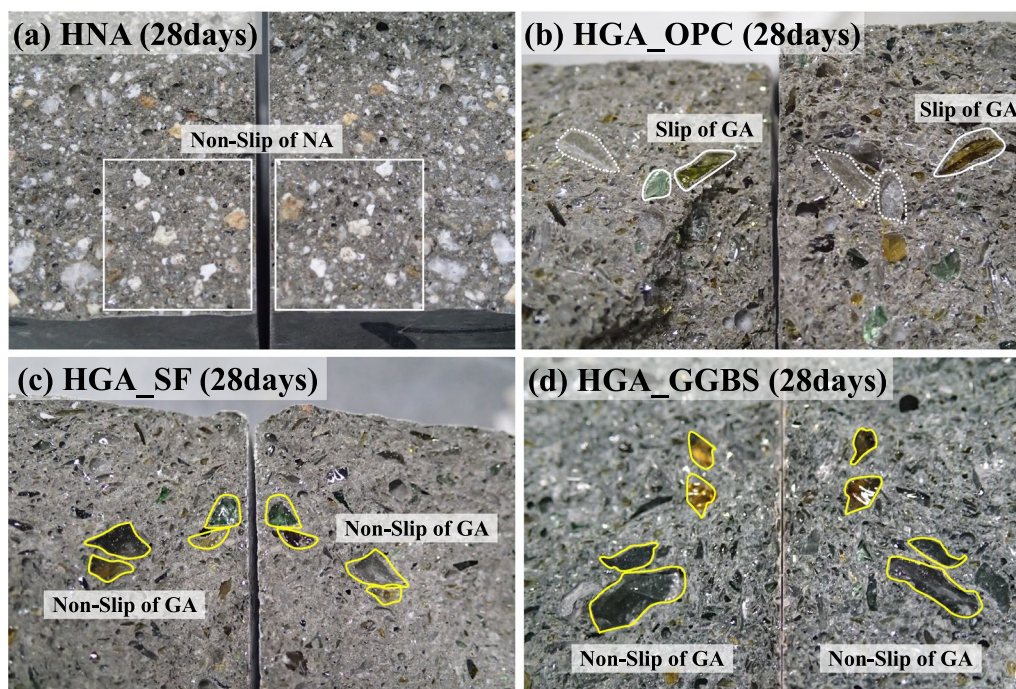


**Fig. 7** Fracture section of high-strength GA mortar after flexural strength test on 28 days; **a** HNA, **b** HGA\_OPC, **c** HGA\_SF, and **d** HGA\_GGBS

aggregates broke apart from the cement matrix, as shown in Fig. 7a. However, as shown in Fig. 7b, when the fracture surface of the HGA\_OPC sample was observed, the GA particles remained intact, suggesting slip in the cement matrix. As shown in Fig. 7c and d, unlike HGA\_OPC, HGS\_SF and GGBS did not cause slipping of the GA. This was due to the increased strength and adhesion of the cement matrix owing to the pozzolanic reaction of SF and GGBS. Meanwhile, HGA\_FA did not show any significant increase in strength owing to its relatively large particle size and slow reactivity compared to those of HGA\_SF and GGBS (Bagheri et al., 2013; Lu et al., 2017). HGA\_FA has been shown to improve long-term mechanical properties owing to its slow pozzolanic reactions.

Accordingly, the effect of SCMs on the flexural strength of the high-strength GA mortar is pronounced. This can be explained by the non-slip shape of the GA. GA has a high fracture strength (approximately 50 MPa) and a long, flat shape. The GA is thought to improve the flexural strength, as it can achieve the crack-bridging effect when a flexural fracture occurs. Therefore, mixing SF and GGBS can improve the mechanical properties of high-strength GA mortars.

### 3.3 ASR

Fig. 8 shows the ASR expansion results obtained using the AMBT. As shown in Fig. 8a, the ASR expansion rate of

NGA\_OPC increases to 0.3%, which exceeds the ASTM limit of 0.2% (after 14 days). It continued to increase, reaching approximately 0.65% after 28 days. In the AMBT environment, excessive ASR expansion occurs because of the reactive silica component of GA. However, the ASR expansion rate of HGA\_OPC was approximately three times higher than that of NGA\_OPC. Despite the high strength, low permeability, and low aggregate/cement ratio of the cement matrix, the ASR expansion rate was very high compared with that of NGA\_OPC. This can be attributed to its dense microstructure (Trägårdh, 1994). Shen et al. also reported that the porous of the mortar may mitigate the ASR gel expansion of GA (Shen et al., 2020). When the ASR begins in NGA\_OPC, the ASR gels can diffuse into the voids, and the buffer effect of the voids accommodating the expansion may appear. In contrast, the dense structure does not accommodate much of the ASR gel and may be more significantly affected by the ASR of GA. In addition, it is reported that the high unit weight of cement may increase the alkalinity of high-strength mortar, which may further increase the ASR of reactive aggregates (Ferraris, 1995).

However, as shown in Fig. 8b, all NGA\_OPC samples with SCMs showed a significant decrease in ASR expansion (Du & Tan, 2013; Duchesne and Bérubé, 1994a, b; Xu et al., 1995). None of the samples exceeded the ASTM C1567 limit of 0.1% (after 14 days). In addition, the HGA samples with SCMs showed significantly reduced ASR

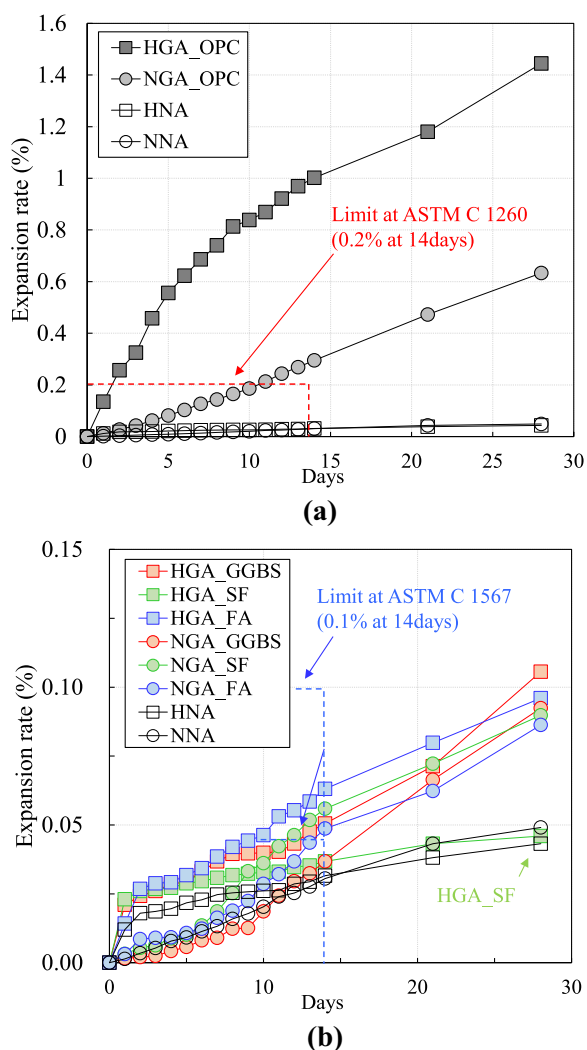


**Fig. 8** The results of ASR expansion rate. **a** NGA\_OPC and HGA\_OPC. **b** NGA\_SCMs and HGA\_SCMs

expansion. None of the HGA\_SCMs samples exceeded the ASTM C1567 limit of 0.1% (after 14 days). HGA\_OPC had a very large ASR expansion, but the ASR expansion rate of the HGA\_SCMs samples was reduced to a degree similar to that of NGA\_SCMs. In particular, HGA\_SF showed the lowest ASR expansion rate (0.046% after 28 days), similar to that of NNA (0.049% after 28 days).

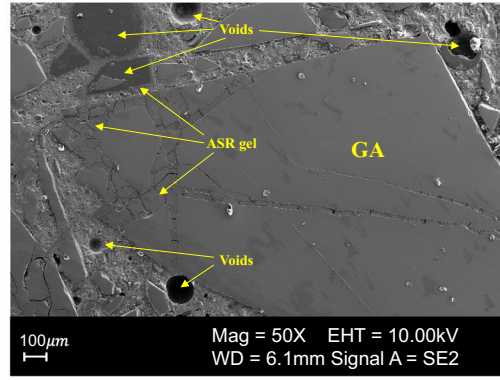
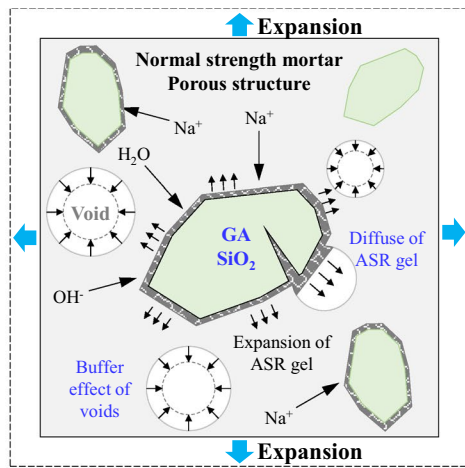
The reason to suppress the ASR expansion by the SCMs can be explained with various reasons. First, pozzolanic reaction of SCMs contributes the reduced permeability of cement paste, and consequently, the mobility of alkali ions in mortar is reduced (Duchesne & Bérubé, 1994a, b; Glasser, 1992; Xu et al., 1995). Second, the pozzolanic reaction by the SCMs provides higher resistance to the expansive stress by ASR gel (Duchesne & Bérubé, 1994a, b; Glasser, 1992). Also, the C–S–H produced by

pozzolanic reaction of SCMs can absorb and entrap a significantly higher quantity of alkali ions than normal C–S–H, thus reducing the quantity of alkali ions and the pH in the pore solution (Glasser, 1992; Hong & Glasser, 1999; Xu et al., 1995). It is judged that these mechanisms of SCMs occur in combination to suppress the ASR expansion of GA. In particular, SF showed the highest ASR expansion reduction effect. This is because SF has the fastest reactivity with alkali ions owing to its micro-particle size (Thomas, 2011).

Fig. 9 shows the differences in the ASR expansion mechanisms and SEM images of each sample after ASR has proceeded for 28 days. For the NGA\_OPC sample, the GA caused ASR expansion. Voids were observed in the microstructure, suggesting that the ASR gel may have diffused through these voids (Fig. 9a). However, the HGA\_OPC sample has fewer pores (Fig. 9b). They are more susceptible to ASR expansion than structures with more pores. As shown in Fig. 9c, FA and GGBS particles were observed in the surroundings of the GA. HGA\_SF did not exhibit visible SF particles because of their small size and complete dissolution. Accordingly, none of HGA\_FA, HGA\_SF, or HGA\_GGBS exhibited an ASR gel in GA, unlike NGA\_OPC or HGA\_OPC. When the HGA\_SCM samples were immersed in NaOH solution, the external Na reacted with the existing SCMs to cause alkaline activation. Additionally, Ca ions in the cement matrix can contribute to the formation of harmful ASR gels (Du & Tan, 2014). SCMs also react with the Ca(OH)<sub>2</sub> in the cement matrix. The SCMs that have reacted with Ca further react with pozzolanic acid to form C–S–H. The C–S–H formed by the SCMs can absorb large amounts of alkali (Monteiro et al., 1997). These complex actions delay the reaction of GA with the alkali ions in GA mortars containing SCMs (Du & Tan, 2014; Monteiro et al., 1997; Xu et al., 1995; Yin et al., 2023).

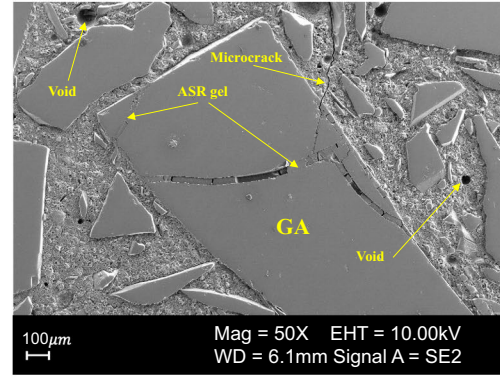
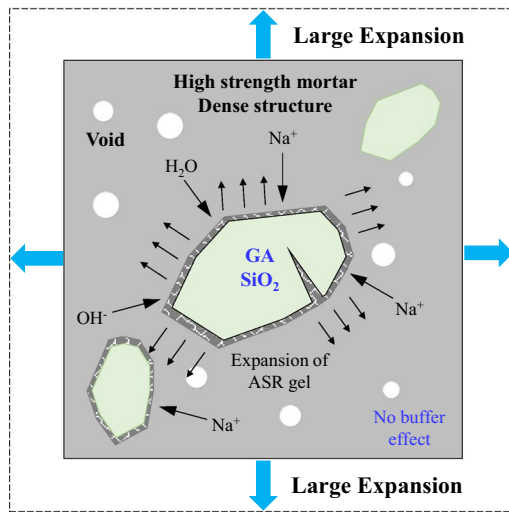
### 3.4 Residual Mechanical Properties After AMBT

The AMBT experimental results indicated that HGA\_OPC exhibited more expansion than NGA\_OPC, and the incorporation of SCMs significantly reduced the ASR expansion in both NGA\_OPC and HGA\_OPC. In this section, the expansion and residual mechanical properties of samples exposed to an AMBT environment are discussed. Fig. 10 shows the ASR expansion after exposure of each specimen to the AMBT environment. Similar to the results of previous experiments, HGA\_OPC showed the largest expansion (1.65% on the 28th day after AMBT), followed by NGA\_OPC (0.84% on the 28th day after AMBT). Additionally, the sample group mixed with SCMs exhibited a relatively small ASR expansion. HGA\_SF showed the smallest ASR expansion (0.08% on the 28th day after AMBT).



**NGA sample after ASR 28days**

(a)



**HGA sample after ASR 28days**

(b)

**Fig. 9** SEM image of samples after ASR 28 days

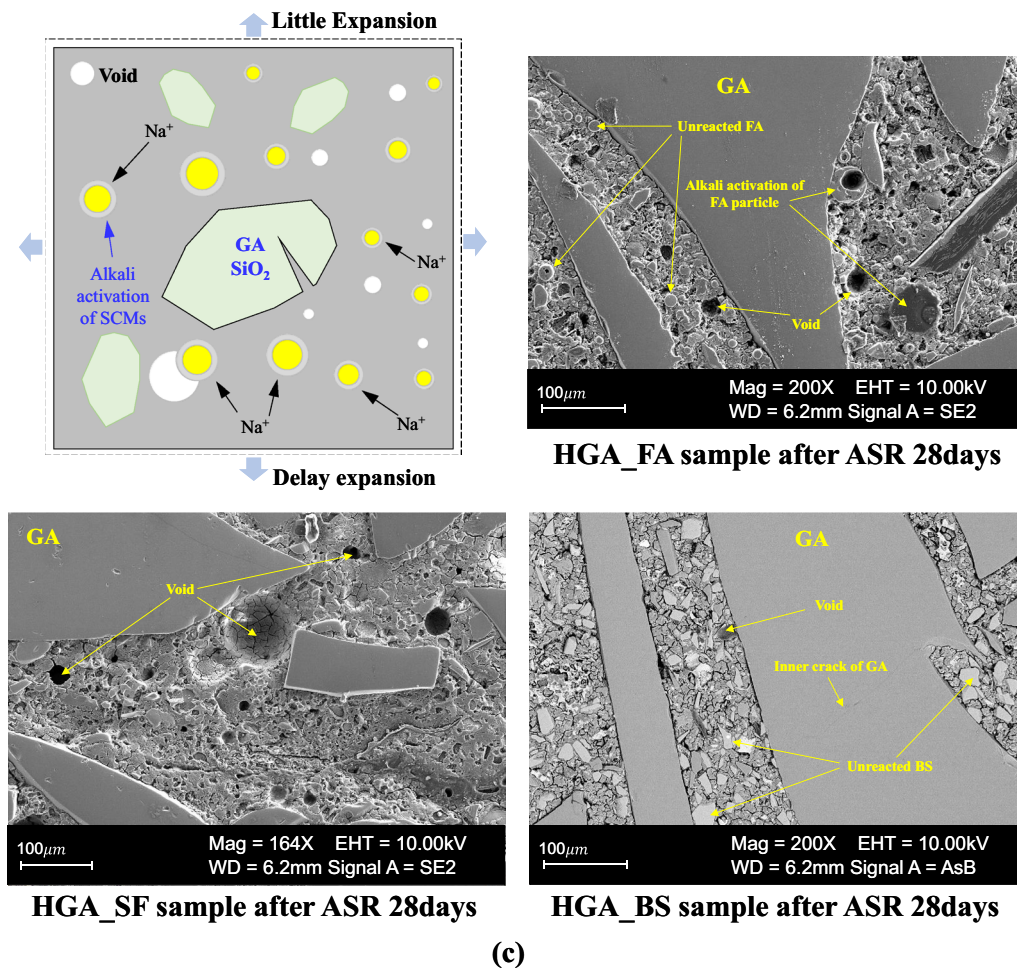


Fig. 9 continued

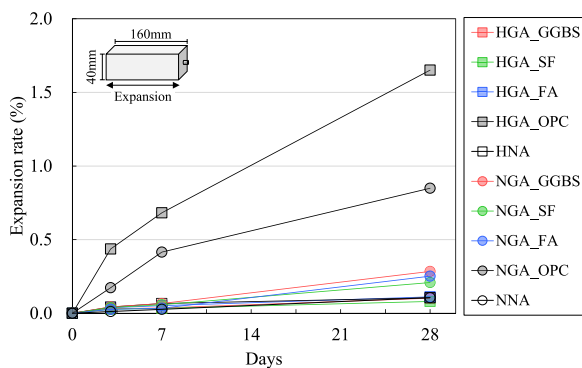
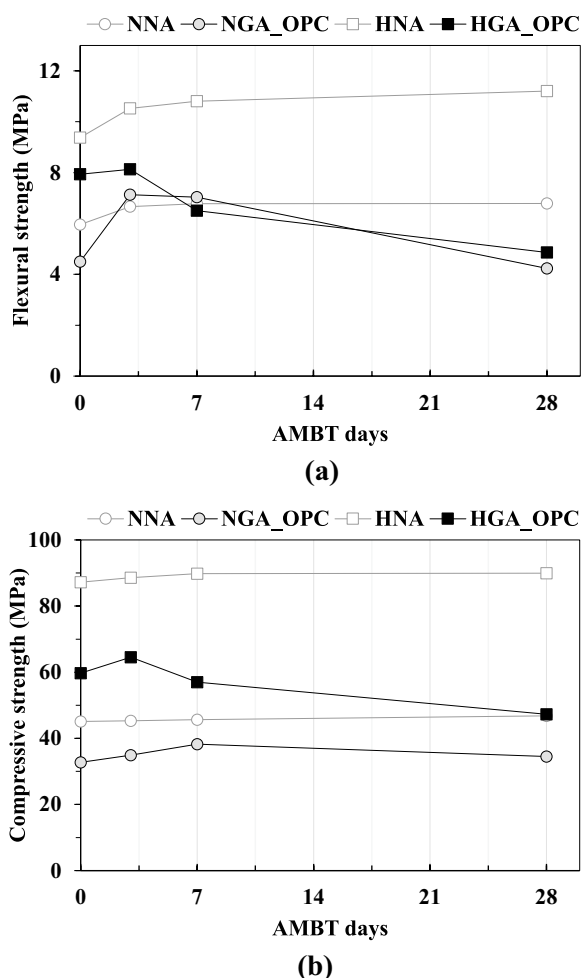


Fig. 10 ASR expansion rate of the residual mechanical properties samples after AMBT

Fig. 11 shows the residual mechanical properties of the NGA\_OPC and HGA\_OPC after AMBT. The residual mechanical properties of the NNA and HNA slightly increased. This can be attributed to the absence of the

ASR in the NA, which may have resulted from the additional hydration reactions of the cement. In the case of NGA\_OPC, the flexural and compressive strengths increased until the 7th day after AMBT. Unlike NGA\_OPC, the residual mechanical properties of HGA\_OPC increased until the 3rd day after AMBT. This is due to the initial ASR of the GA. The ASR of the early GA can improve the ITZ between the GA and cement interface, and the ASR gel fills the voids (Lu et al., 2017). Fig. 12 presents the SEM analysis results of the GA and ITZ before and 7 days after AMBT. Before AMBT, a gap of approximately 2.3 µm existed between the GA and cement matrix (Fig. 12a). These gaps could reduce the adhesion strength between the GA and cement matrix, consequently affecting the mechanical properties. However, on the 7th day after AMBT, ASR products were formed on the surface of several GA particles, leading to a reduction in the ITZ size (Fig. 12b). Even small GA particles reacted and contributed to filling the matrix.



**Fig. 11** Residual mechanical properties after AMBT of NGA\_OPC and HGA\_OPC. **a** Residual flexural strength. **b** Residual compressive strength

Meanwhile, during continuous AMBT, NGA\_OPC began to exhibit a decrease in residual mechanical properties on the 28th day after AMBT. In particular, a significant reduction in the residual flexural strength was observed. This reduction in residual flexural strength is attributed to the excessive ASR expansion of GA (Jones & Clark, 1996; Siemes & Visser, 2000; Takemura et al., 1996). Continuous ASR expansion causes cracks in the cement matrix and reduces mortar strength. In the case of the GA, the strength may be further reduced by the destruction and damage to the GA due to the ASR occurring inside the GA. The compressive strength does not decrease as significantly as the flexural strength. Hans et al. also reported that ASR does not appear to impact compressive strength (Reinhardt et al., 2018). In contrast, the residual mechanical properties of HGA\_OPC decreased when measured on the 7th day after AMBT. The residual mechanical properties of HGA\_OPC after

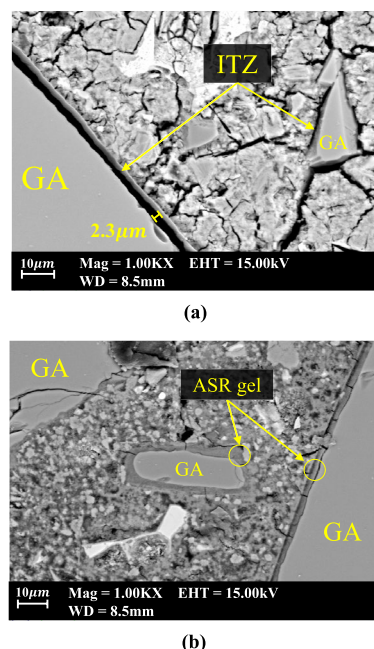


**Fig. 12** SEM image of NGA\_OPC sample before and after AMBT; **a** ITZ of GA and cement matrix, **b** ASR gel formation at ITZ of GA

AMBT tended to decrease more rapidly and significantly than those of NGA\_OPC. This could be attributed to HGA\_OPC experiencing faster ASR expansion than NGA\_OPC.

Fig. 13 shows the residual mechanical properties of the NGA and HGA with SCMs after AMBT. The residual flexural and compressive strengths of NGA\_FA, GGBS, HGA\_FA, and GGBS increased until the 3rd day after AMBT. NGA\_SF and HGA\_SF exhibited a tendency toward increased residual flexure and compressive strength for up to 7 days after AMBT. During this period, no ASR expansion was observed in the mortar (Fig. 10). This indicates that SCMs encounter alkali ions and undergo alkali activation and pozzolanic reactions. However, on the 28th day after AMBT, most of the samples showed a decrease in residual flexural and compressive strengths. What is noteworthy here is the reduction in flexural strength after 28 days of keeping the mortar under AMBT conditions, despite the lower ASR expansion.

In the case of the GA mortar incorporating SCMs, the decrease in residual flexural strength after 28 days post-AMBT, despite the low ASR expansion, was attributed to ASR-induced damage in the GA due to surface cracking. An SEM analysis was conducted to investigate this phenomenon. As shown in Fig. 14, most specimens with SCMs exhibited GA destruction caused by the ASR gel. In the previous discussions, it was suggested that the

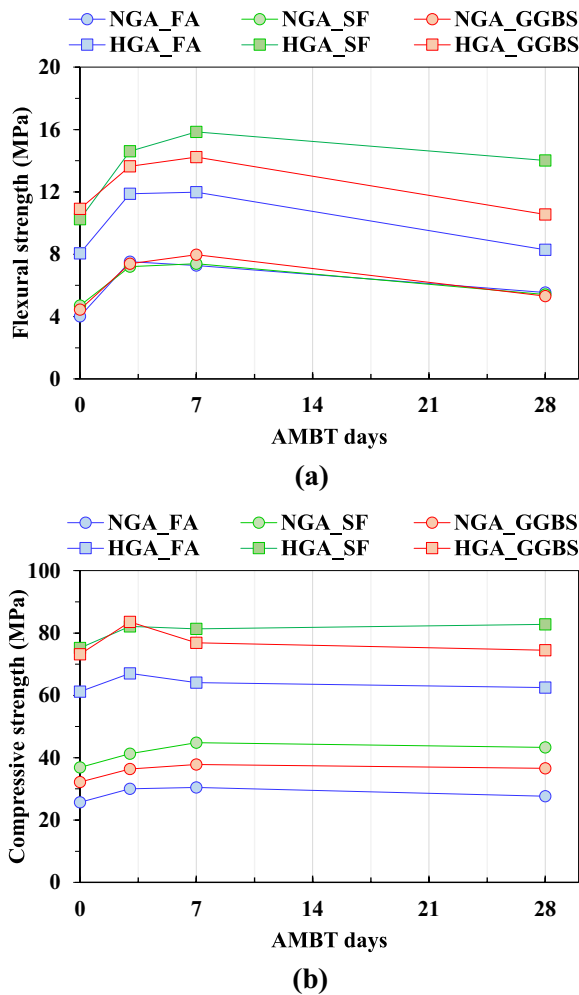


**Fig. 13** Residual mechanical properties after AMBT of GA mortar with SCMs' samples. **a** Residual flexural strength. **b** Residual compressive strength

delayed occurrence of the ASR in GA could be attributed to the alkali activation and pozzolanic reaction of SCMs with alkaline ions and Ca in the cement matrix. However, in harsh environments with continuous alkali exposure, such as the AMBT, an internal ASR was observed within the GA. Similarly, Maraghechi et al., (2016) reported internal ASR was occurred in the GA of alkali-activated FA mortar that did not form expansive ASR gels. This was attributed to the CaO content of GA and the presence of microcracks on the surface. These fine cracks led to more internal ASR in the GA than surface ASR, as previously reported (Du & Tan, 2014; Sun et al., 2021). The surface ASR gel is formed by reacting with Ca to create a secondary C-S-H layer, whereas the ASR within the fine cracks in the GA expands inward, providing new sites for

ASR occurrence (Du & Tan, 2014). Consequently, the GA suffered more significant deterioration owing to these internal ASR gel. Therefore, in the GA mortar containing SCMs, the internal ASR within the GA resulted in the deterioration of strength, even though the SCMs delayed the ASR expansion. Ultimately, the removal or mitigation of surface cracks in GA can serve as a crucial method for preventing GA deterioration caused by the ASR, thereby enhancing the ASR resistance of GA mortar. In contrast, as illustrated in Fig. 14e, HGA\_SF showed minor GA cracking in some areas, but no severe damage from the ASR was observed. Accordingly, as observed in Fig. 13, it displayed the least degradation in the residual flexural and compressive strengths among all mortars.

Fig. 15 summarizes the causes of the strength increase and decrease in the GA mortar due to the AMBT. Initially, the residual strength of the GA mortar increased during the early stages of AMBT, owing to the charging effect of the initial ASR gel of the GA. ASR simultaneously causes the deterioration of the GA and mortar strength reduction owing to expansion. However, the GA mortar incorporating SCMs, unlike NGA\_OPC and HGA\_OPC, exhibited a dominance of the pozzolanic reaction and alkali activation during the early stages of AMBT. It is likely that the ASR in the GA was also active during this period. Consequently, the residual strength of GA mortar with SCMs increased significantly due to these phenomena. However, when the pozzolanic reaction and alkali activation of SCMs progress to a certain extent, ASR in GA begins to occur, leading to a reduction in the residual mechanical properties.

To analyze these phenomena quantitatively, the  $f_{IS}$  and  $f_{DS}$  values for each specimen were calculated.  $f_{IS}$  and  $f_{DS}$  were determined using Eqs. (1) and (2), respectively. Equation (1) is expressed as follows:

$$f_{IS} = (f_{max} - f_i) / f_i \times 100 \quad (1)$$

where  $f_{IS}$  is the residual relative strength increase (%),  $f_{max}$  is the maximum residual strength (MPa), and  $f_i$  is the initial strength before AMBT (MPa). Equation (2) is expressed as follows:

$$f_{DS} = (f_{max} - f_{AMBT}^{28}) / f_{max} \times 100, \quad (2)$$

where  $f_{DS}$  is the residual relative decreasing strength (%),  $f_{max}$  is the maximum residual strength (MPa), and  $f_{AMBT}^{28}$  is the residual strength 28 days after AMBT (MPa).

The results of  $f_{IS}$  and  $f_{DS}$  for the residual flexural and compressive strengths are presented in Fig. 16. NNA and HNA exhibited very low  $f_{IS}$  and  $f_{DS}$ , because they

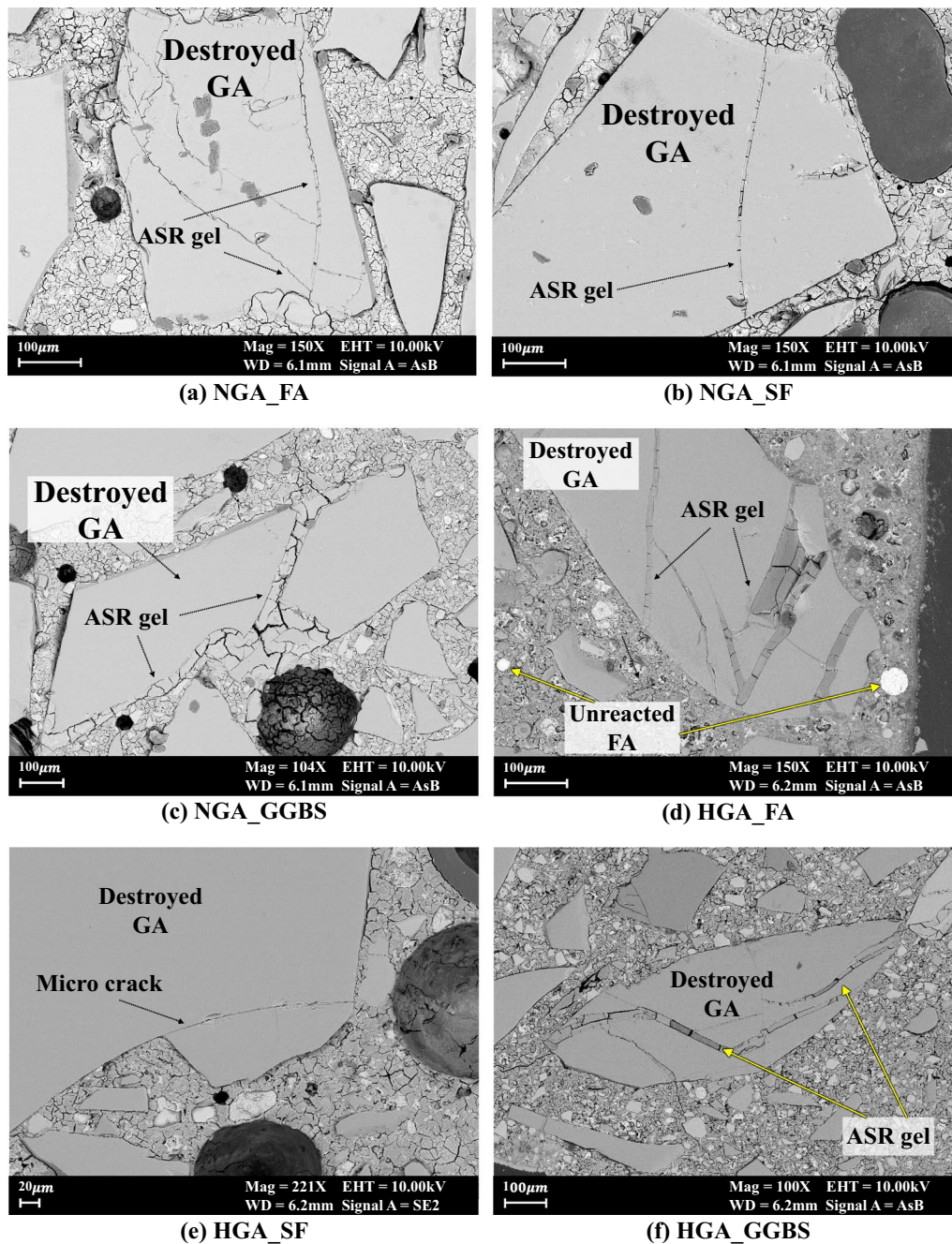
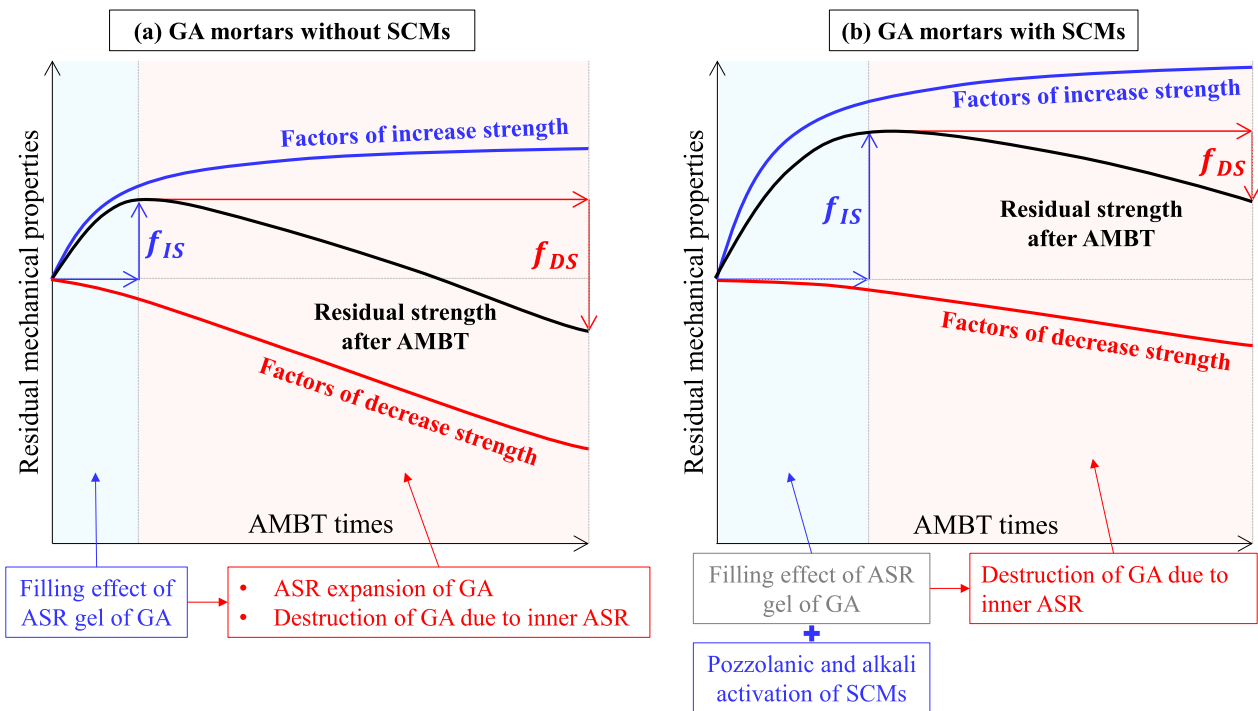


Fig. 14 SEM and BSE image 28 days after AMBT of GA mortar with SCMs' samples

did not undergo ASR. Meanwhile, NGA\_OPC exhibited a 60% increase in flexural strength and a 17% increase in compressive strength. The  $f_{IS}$  values of NGA\_FA, SF, and GGBS varied slightly among the specimens but were generally higher than the  $f_{IS}$  values of NGA\_OPC. This was attributed to the alkali activation of the SCMs.

In addition, the  $f_{DS}$  values of NGA\_FA, SF, and GGBS were lower than those of NGA\_OPC. In contrast, HGA exhibited lower  $f_{IS}$  values owing to the rapid ASR expansion compared with the other specimens. However, its  $f_{DS}$  value was very high, indicating a rapid decrease in the residual strength. HGA\_FA, SF, and GGBS showed increased  $f_{IS}$  and decreased  $f_{DS}$  values compared with



**Fig. 15** Schematic of residual mechanical properties behavior according to presence SCMs in GA mortars

HGA\_OPC because of the alkali activation of the SCMs. In particular, HGA\_SF's flexural strength  $f_{DS}$  was very low, and its compressive strength did not decrease.

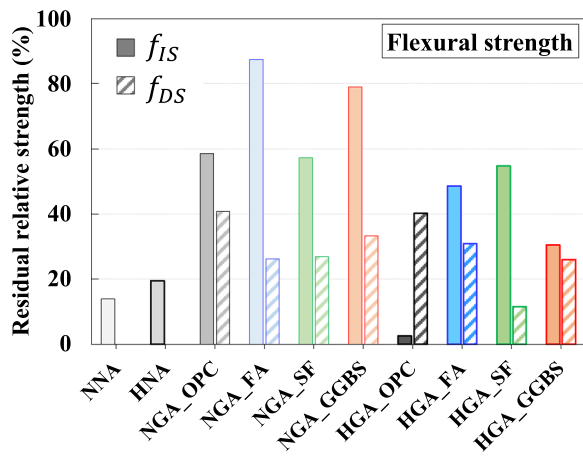
An analysis of the correlation between  $f_{DS}$  values and the ASR expansion is shown in Fig. 17. As shown in Fig. 17, a proportional relationship between ASR expansion and  $f_{DS}$  for strength was confirmed. As shown in Fig. 17a, GA mortar incorporating SCMs exhibited high flexural strength  $f_{DS}$  values (25–33%) despite low ASR expansion. In contrast, as depicted in Fig. 17b, GA mortar with SCMs exhibited relatively low compressive strength  $f_{DS}$  values (3–12%) at low ASR expansion. This suggests that the ASR-induced damage has a greater impact on the flexural strength than on the compressive strength. Notably, HGA\_SF displayed the lowest expansion and  $f_{DS}$  values for both the flexural and compressive strengths. Previous studies have suggested that the use of FA and GGBS can effectively improve ASR by forming non-expansive ASR gels with high Al/Si and low Ca/Si ratios owing to their aluminum content (Khan et al., 2021). However, SF, which has a very low aluminum content and highly reactive amorphous silica particles,

is known to have higher reactivity than FA and GGBS (Thomas, 2011). Consequently, SF can rapidly react with external alkali ions, effectively delaying the ASR in GAs. In particular, in the dense structure of high-strength mortar, the pozzolanic reaction of SF may further enhance the ASR expansion and penetration resistances. Therefore, the use of SF in a high-strength cement matrix is considered effective for controlling the ASR of GAs and maintaining their performance. When GA is used in ultra-high-performance concrete (UHPC) or high-strength cementitious compositions, the use of SF may facilitate ASR control and mitigate the degradation of mechanical properties.

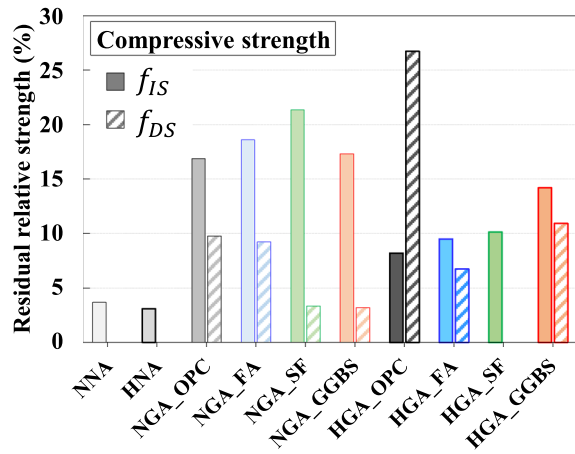
#### 4 Conclusion

This study evaluated the mechanical properties and ASR expansion behavior of high- and normal-strength mortar incorporating 100% waste glass fine aggregate as well as fly ash, blast furnace slag, or silica fume as a supplementary cementitious material. The accelerated mortar bar test (AMBT) was used to induce ASR. In addition, the





(a)

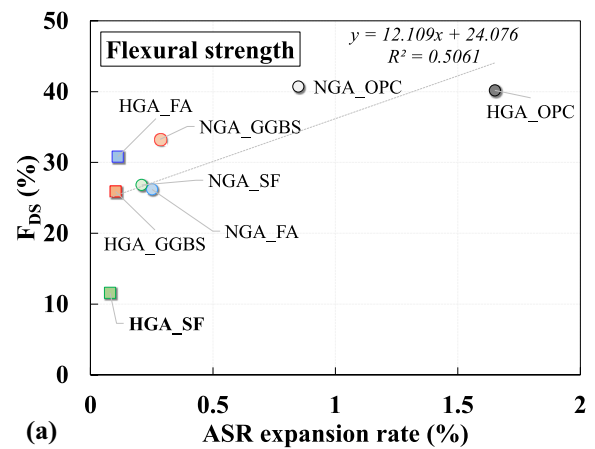


(b)

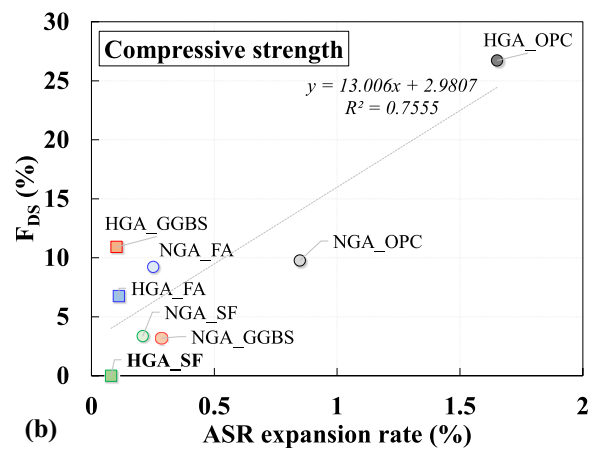
**Fig. 16** Rate of change of residual mechanical properties of samples. **a** Residual flexural strength. **b** Residual compressive strength

residual mechanical properties of the high-strength GA mortar were analyzed under AMBT conditions. The conclusions are as follows:

- Both normal- and high-strength GA mortars exhibited a decrease in mechanical properties compared to the natural fine aggregate mortar. Slipping of the GA was also observed in both the normal- and high-strength cement matrices. However, the incorporation of highly reactive SF and GGBS can improve both the degradation of the mechanical properties and the slip of GA in high-strength GA mortars.



(a)



(b)

**Fig. 17** Relationship between ASR expansion rate and  $f_{DS}$ . **a**  $f_{DS}$  of Flexural strength. **b**  $f_{DS}$  of compressive strength

- AMBT performed on the high-strength GA mortar revealed that the ASR expansion of GA was approximately three times higher than that of the normal-strength GA mortar, which was attributed to its dense, non-porous structure. As a result, the residual mechanical properties degraded more rapidly than those of the normal-strength GA mortar.
- Owing to the pozzolanic reaction of SCMs, that is, FA, SF, and GGBS, their incorporation into both normal and high-strength GA mortar significantly reduced the ASR expansion rate and did not cause any significant decrease in the residual mechanical properties. However, for the high-strength mortar, despite the low ASR expansion rates, exposure to the AMBT environment results in the deterioration

of GA owing to the inner ASR, causing a significant decrease in the flexural strength of the GA mortar.

- The incorporation of SF in high-strength GA mortar resulted in minimal ASR expansion and significantly improved the residual mechanical properties of the high- and normal-strength mortars. SF demonstrated the most effective delay in ASR expansion in high-strength GA mortars. Consequently, it is suggested that GA can be employed in UHPC or high-strength cement composites, where SF is more commonly utilized. However, further testing of other properties is required to confirm its applicability.

This study confirms that even in the presence of SCMs, the performance of the GA may deteriorate owing to the ASR originating from surface cracks under harsh AMBT conditions. Further research on surface modification and coating to eliminate surface cracks in GA is anticipated to improve its performance against ASR-induced degradation. Additionally, long-term performance-monitoring experiments on high-strength GA mortars are necessary for a more comprehensive understanding.

#### Acknowledgements

Not applicable.

#### Author contributions

Hamin Eu contributed to conceptualization, methodology, experiment execution, data analysis, and writing—original draft; Gyuyong Kim contributed to funding acquisition, supervision, project administration, resources, and validation; Minjae Son contributed to validation, and writing—review and editing; Sasui Sasui contributed to validation and writing—review and editing; Yaechan Lee contributed to experiment execution and data interpretation; Hyeonggil Choi, and Sukpyo Kang contributed to writing—review and editing; Jeongsoo Nam contributed to resources and supervision. All the authors read and approved the final manuscript.

#### Funding

This work was supported by the National Research Foundation of Korea (NRF) grant funded by the Korea government (MSIT) (No. RS-2023-00220921) and BK21 FOUR Program by Chungnam National University Research Grant, 2022.

#### Availability of data and materials

The datasets used and/or analyzed during the current study are available from the corresponding author on reasonable request.

#### Declarations

#### Competing interests

The authors declare that they have no competing interests.

#### Author details

<sup>1</sup>Department of Architectural Engineering, Chungnam National University, Daejeon 34134, Republic of Korea. <sup>2</sup>Department of Future & Smart Construction Research, Korea Institute of Civil Engineering and Building Technology, 283, Goyang-Daero, Ilsanseo-Gu, Goyang-Si 10223, Republic of Korea. <sup>3</sup>School of Architecture, Kyungpook National University, Daegu 41566, Republic of Korea. <sup>4</sup>Department of Architectural Engineering, Woosuk University, Jincheon 27841, Republic of Korea.

Received: 23 February 2024 Accepted: 26 June 2024

Published online: 08 October 2024

#### References

- Ahmad, J., Martinez-Garcia, R., Algarni, S., de Prado-Gil, J., Alqahtani, T., & Irshad, K. (2022). Characteristics of sustainable concrete with partial substitutions of glass waste as a binder material. *International Journal of Concrete Structures and Materials*, 16(1), 1–18. <https://doi.org/10.1186/s40069-022-00511-1>
- ASTM C1260–22. (2014). Standard test method for potential alkali reactivity of aggregates (Mortar-Bar Method). *ASTM International*. <https://doi.org/10.1520/C1260-22.2>
- ASTM C1293. (2015). Standard test method for determination of length change of concrete due to alkali-silica reaction. *Annual Book of ASTM Standards*. <https://doi.org/10.1520/C1293-20A.2>
- ASTM C1567–04. (2005). Standard test method for determining the potential alkali-silica reactivity of combinations of cementitious materials and aggregate (Accelerated Mortar-Bar Method). *Annual Book of ASTM Standards*, 04(02), 774–778. <https://doi.org/10.1520/C1567-21>
- ASTM C33/C33M–18. (2010). Standard specification for concrete aggregates. *ASTM International, i(C)*, 1–11. <https://doi.org/10.1520/C0033>
- ASTM C 490. (2017). Standard practice for use of apparatus for the determination of length change of hardened cement paste, mortar, and concrete. *ASTM International, 1*, 1–5. <https://doi.org/10.1520/C0490>
- Bagheri, A., Zanganeh, H., Alizadeh, H., Shakerinia, M., & Marian, M. A. S. (2013). Comparing the performance of fine fly ash and silica fume in enhancing the properties of concretes containing fly ash. *Construction and Building Materials*, 47, 1402–1408. <https://doi.org/10.1016/j.conbuildmat.2013.06.037>
- Cement-Test Methods-Determination of Strength. (2009). Geneva: International Organization for Standardization.
- Corinaldesi, V., Gnappi, G., Moriconi, G., & Montenero, A. (2005). Reuse of ground waste glass as aggregate for mortars. *Waste Management*, 25(2 SPEC. ISS), 197–201. <https://doi.org/10.1016/j.wasman.2004.12.009>
- Drzymala, T., Zegardlo, B., & Tofilo, P. (2020). Properties of concrete containing recycled glass aggregates produced of exploded lighting materials. *Materials*, 13(1), 1–16. <https://doi.org/10.3390/ma13010226>
- Du, S., Zhao, Q., & Shi, X. (2021). High-volume fly ash-based cementitious composites as sustainable materials: An overview of recent advances. *Advances in Civil Engineering*. <https://doi.org/10.1155/2021/4976169>
- Du, H., & Tan, K. H. (2013). Use of waste glass as sand in mortar: Part II—Alkali-silica reaction and mitigation methods. *Cement and Concrete Composites*, 35(1), 118–126. <https://doi.org/10.1016/j.cemconcomp.2012.08.029>
- Du, H., & Tan, K. H. (2014). Effect of particle size on alkali-silica reaction in recycled glass mortars. *Construction and Building Materials*, 66, 275–285. <https://doi.org/10.1016/j.conbuildmat.2014.05.092>
- Du, H., & Tan, K. H. (2017). Properties of high volume glass powder concrete. *Cement and Concrete Composites*, 75, 22–29. <https://doi.org/10.1016/j.cemconcomp.2016.10.010>
- Duchesne, J., & Bérubé, M. A. (1994a). The effectiveness of supplementary cementing materials in suppressing expansion due to ASR: Another look at the reaction mechanisms part 2: Pore solution chemistry. *Cement and Concrete Research*, 24(2), 221–230. [https://doi.org/10.1016/0008-8846\(94\)90047-7](https://doi.org/10.1016/0008-8846(94)90047-7)
- Duchesne, J., & Bérubé, M. A. (1994b). The effectiveness of supplementary cementing materials in suppressing expansion due to ASR: Another look at the reaction mechanisms part 1: Concrete expansion and portlandite depletion. *Cement and Concrete Research*, 24(1), 73–82.
- EN 1015–7: 2007. Methods of test for mortar masonry—part 7: Determination of air content of fresh mortar.
- Ferraris CF. (1995). Alkali-silica reaction and high performance concrete.24. <http://fire.nist.gov/bfrlpubs/build95/art004.html>
- Giaccio, G., Zerbino, R., Ponce, J. M., & Batic, O. R. (2008). Mechanical behavior of concretes damaged by alkali-silica reaction. *Cement and Concrete Research*, 38(7), 993–1004. <https://doi.org/10.1016/j.cemconres.2008.02.009>
- Glasser, F. P. (1992). *Chemistry of the alkali-aggregate reaction. Chap 2, the Alkali-Silica Reaction in Concrete*. New York: Swamy R.N.
- Hajighasemali, S., Ramezani-pour, A., & Kashefzadeh, M. (2014). The effect of alkali-silica reaction on strength and ductility analyses of RC beams. *Magazine of Concrete Research*, 66(15), 751–760. <https://doi.org/10.1680/macr.13.00282>
- Hamada, H., Alattar, A., Tayeh, B., Yahaya, F., & Thomas, B. (2022). Effect of recycled waste glass on the properties of high-performance concrete:

- A critical review. *Case Studies in Construction Materials*, 17(May), e01149. <https://doi.org/10.1016/j.cscm.2022.e01149>
- Hong, S. Y., & Glasser, F. P. (1999). Alkali binding in cement pastes: Part I. The C-S-H phase. *Cement and Concrete Research*, 29(12), 1893–1903. [https://doi.org/10.1016/S0008-8846\(99\)00187-8](https://doi.org/10.1016/S0008-8846(99)00187-8)
- Jiao, Y., Zhang, Y., Guo, M., Zhang, L., Ning, H., & Liu, S. (2020). Mechanical and fracture properties of ultra-high performance concrete (UHPC) containing waste glass sand as partial replacement material. *Journal of Cleaner Production*, 277, 123501. <https://doi.org/10.1016/j.jclepro.2020.123501>
- Jones, A. E., & Clark, L. A. (1996). A review of the Institution of Structural Engineers report: "Structural effects of alkali-silica reaction (1992)." In International Conference on Alkali-Aggregate Reaction in Concrete, 10th, 1996, Melbourne, Victoria, Australia (pp. 394–401).
- Khan, M. N. N., Saha, A. K., & Sarker, P. K. (2021). Evaluation of the ASR of waste glass fine aggregate in alkali activated concrete by concrete prism tests. *Construction and Building Materials*, 266, 121121. <https://doi.org/10.1016/j.conbuildmat.2020.121121>
- Kou, S. C., & Poon, C. S. (2009). Properties of self-compacting concrete prepared with recycled glass aggregate. *Cement and Concrete Composites*, 31(2), 107–113. <https://doi.org/10.1016/j.cemconcomp.2008.12.002>
- Koyanagi, W., Rokugo, K., & Ishida, H. (1986). Failure behavior of reinforced concrete beams deteriorated by alkali-silica reactions. In Proc. 7th Int. Conf. on AAR. Ottawa.
- Kwan, W. H., Ramli, M., Kam, K. J., & Sulieman, M. Z. (2012). Influence of the amount of recycled coarse aggregate in concrete design and durability properties. *Construction and Building Materials*, 26(1), 565–573. <https://doi.org/10.1016/j.conbuildmat.2011.06.059>
- Larive C, Laplaud A, Joly M. Behavior of AAR-affected concrete: Experimental data. In Proc., 10th Int. Conf. on AAR 1996 Aug (pp. 670-677). Melbourne, Australia.
- Lu, J. X., Zhan, B. J., Duan, Z. H., & Poon, C. S. (2017). Improving the performance of architectural mortar containing 100% recycled glass aggregates by using SCMs. *Construction and Building Materials*, 153, 975–985. <https://doi.org/10.1016/j.conbuildmat.2017.07.118>
- Maraghechi, H., Rajabipour, F., Pantano, C. G., & Burgos, W. D. (2016). Effect of calcium on dissolution and precipitation reactions of amorphous silica at high alkalinity. *Cement and Concrete Research*, 87, 1–13. <https://doi.org/10.1016/j.cemconres.2016.05.004>
- Mohammadi, A., Ghiasvand, E., & Nili, M. (2020). Relation between mechanical properties of concrete and alkali-silica reaction (ASR): a review. *Construction and Building Materials*, 258, 119567. <https://doi.org/10.1016/j.conbuildmat.2020.119567>
- Monteiro, P. J. M., Wang, K., Sposito, G., Dos Santos, M. C., & De Andrade, W. P. (1997). Influence of mineral admixtures on the alkali-aggregate reaction. *Cement and Concrete Research*, 27(12), 1899–1909. [https://doi.org/10.1016/S0008-8846\(97\)00206-8](https://doi.org/10.1016/S0008-8846(97)00206-8)
- Omran, A. F., Etienne, D. M., Harbec, D., & Tagnit-Hamou, A. (2017). Long-term performance of glass-powder concrete in large-scale field applications. *Construction and Building Materials*, 135, 43–58. <https://doi.org/10.1016/j.conbuildmat.2016.12.218>
- Padmini, A. K., Ramamurthy, K., & Mathews, M. S. (2009). Influence of parent concrete on the properties of recycled aggregate concrete. *Construction and Building Materials*, 23(2), 829–836. <https://doi.org/10.1016/j.conbuildmat.2008.03.006>
- Park, S. B., & Lee, B. C. (2004). Studies on expansion properties in mortar containing waste glass and fibers. *Cement and Concrete Research*, 34(7), 1145–1152. <https://doi.org/10.1016/j.cemconres.2003.12.005>
- Rashad, A. M. (2014). Recycled waste glass as fine aggregate replacement in cementitious materials based on Portland cement. *Construction and Building Materials*, 72, 340–357. <https://doi.org/10.1016/j.conbuildmat.2014.08.092>
- Reinhardt, H. W., Özkan, H., & Mielich, O. (2018). Changes in mechanical properties of concrete due to ASR (Cambios en las propiedades mecánicas del hormigón debido a la ASR). *Hormigón y Acero*, 69, 15–19.
- Sasui, S., Kim, G., Nam, J., van Riessen, A., Eu, H., Chansomsak, S., et al. (2020). Incorporation of waste glass as an activator in Class-C Fly Ash/GGBS based Alkali activated material. *Materials*. <https://doi.org/10.3390/ma13173906>
- Sasui, S., Kim, G., Nam, J., van Riessen, A., Hadzima-Nyarko, M., Choe, G., et al. (2022). Effects of waste glass sand on the thermal behavior and strength of fly ash and GGBS based alkali activated mortar exposed to elevated temperature. *Construction and Building Materials*, 316(August 2021), 125864. <https://doi.org/10.1016/j.conbuildmat.2021.125864>
- Sasui, S., Kim, G., Nam, J., Alam, S. F., Eu, H., Lee, Y., & Ahmad, M. (2023). Alkali activation of waste concrete powder: Effects of alkali type and concentration. *Ceramics International*. <https://doi.org/10.1016/j.ceramint.2023.01.224>
- Sasui, S., Kim, G., Nam, J., van Riessen, A., & Hadzima-Nyarko, M. (2021). Effects of waste glass as a sand replacement on the strength and durability of fly ash/GGBS based alkali activated mortar. *Ceramics International*, 47(15), 21175–21196. <https://doi.org/10.1016/j.ceramint.2021.04.121>
- Shayan, A., & Xu, A. (2004). Value-added utilisation of waste glass in concrete. *Cement and Concrete Research*, 34(1), 81–89. [https://doi.org/10.1016/S0008-8846\(03\)00251-5](https://doi.org/10.1016/S0008-8846(03)00251-5)
- Shayan, A., & Xu, A. (2006). Performance of glass powder as a pozzolanic material in concrete: A field trial on concrete slabs. *Cement and Concrete Research*, 36(3), 457–468. <https://doi.org/10.1016/j.cemconres.2005.12.012>
- Shen, P., Zheng, H., Liu, S., Lu, J. X., & Poon, C. S. (2020). Development of high-strength pervious concrete incorporated with high percentages of waste glass. *Cement and Concrete Composites*, 114(August), 103790. <https://doi.org/10.1016/j.cemconcomp.2020.103790>
- Shi, C., Wu, Y., Riefler, C., & Wang, H. (2005). Characteristics and pozzolanic reactivity of glass powders. *Cement and Concrete Research*, 35(5), 987–993. <https://doi.org/10.1016/j.cemconres.2004.05.015>
- Siemes, A. J. M., & Visser, J. H. M. (2000). Low tensile strength in older concrete structures with alkali-silica reaction. In Proceedings 11th International Conference on Alkali-Aggregate Reaction (ICAAAR), Québec, Canada. 1029–1038
- Soliman, N. A., & Tagnit-Hamou, A. (2017). Using glass sand as an alternative for quartz sand in UHPC. *Construction and Building Materials*, 145, 243–252. <https://doi.org/10.1016/j.conbuildmat.2017.03.187>
- Sun, L., Zhu, X., Kim, M., & Zi, G. (2021). Alkali-silica reaction and strength of concrete with pretreated glass particles as fine aggregates. *Construction and Building Materials*, 271, 121809. <https://doi.org/10.1016/j.conbuildmat.2020.121809>
- Tabsh, S. W., & Abdelfatah, A. S. (2009). Influence of recycled concrete aggregates on strength properties of concrete. *Construction and Building Materials*, 23(2), 1163–1167. <https://doi.org/10.1016/j.conbuildmat.2008.06.007>
- Taha, B., & Nounu, G. (2009). Utilizing waste recycled glass as sand/cement replacement in concrete. *Journal of Materials in Civil Engineering*, 21(12), 709–721. [https://doi.org/10.1061/\(asce\)0899-1561\(2009\)21:12\(709\)](https://doi.org/10.1061/(asce)0899-1561(2009)21:12(709))
- Takemura, K., Ichitubo, M., Tazawa, E., & Yonekura, A. (1996). Mechanical performance of ASR affected nearly full-scale reinforced concrete columns. In International Conference on Alkali-Aggregate Reaction in Concrete, 10th, 1996, Melbourne, Victoria, Australia.
- Tan, K. H., & Du, H. (2013). Use of waste glass as sand in mortar: Part I—Fresh, mechanical and durability properties. *Cement and Concrete Composites*, 35(1), 109–117. <https://doi.org/10.1016/j.cemconcomp.2012.08.028>
- Thomas, M. (2011). The effect of supplementary cementing materials on alkali-silica reaction: A review. *Cement and Concrete Research*, 41(12), 1224–1231. <https://doi.org/10.1016/j.cemconres.2010.11.003>
- Tittarelli, F., Giosuè, C., & Mobili, A. (2018). Recycled glass as aggregate for architectural mortars. *International Journal of Concrete Structures and Materials*. <https://doi.org/10.1186/s40069-018-0290-3>
- Trägårdh, J. (1994). Alkali-silica reaction in high strength concrete
- Xu, G. J. Z., Watt, D. F., & Hudec, P. P. (1995). Effectiveness of mineral admixtures in reducing ASR expansion. *Cement and Concrete Research*, 25(6), 1225–1236. [https://doi.org/10.1016/S0008-8846\(95\)00115-5](https://doi.org/10.1016/S0008-8846(95)00115-5)
- Yin, W., Li, X., Chen, Y., Wang, Y., Xu, M., & Pei, C. (2023). Mechanical and rheological properties of High-Performance concrete (HPC) incorporating waste glass as cementitious material and fine aggregate. *Construction and Building Materials*, 387(December 2022), 131656. <https://doi.org/10.1016/j.conbuildmat.2023.131656>

### **Publisher's Note**

Springer Nature remains neutral with regard to jurisdictional claims in published maps and institutional affiliations.

**Hamin Eu** is Doctoral course student in Department of Architectural Engineering, College of Engineering at Chungnam National University, Daejeon, Republic of Korea.

**Gyuyong Kim** is Professor in Department of Smart City Architectural Engineering, College of Engineering at Chungnam National University, Daejeon, Republic of Korea.

**Minjae Son** is ph.D in Department of Future & Smart Construction Research, Korea Institute of Civil Engineering and Building Technology, Goyang, Republic of Korea.

**Sasui Sasui** is research professor in Department of Architectural Engineering, College of Engineering at Chungnam National University, Daejeon, Republic of Korea.

**Yaechan Lee** is Doctoral course student in Department of Architectural Engineering, College of Engineering at Chungnam National University, Daejeon, Republic of Korea.

**Hyeonggil Choi** is Assistant Professor in School of Architecture, College of Engineering at Kyungpook National University, Daegu, Republic of Korea.

**Sukpyo Kang** is Professor in Department of Architectural Engineering, Woosuk University, Jincheon, Republic of Korea.

**Jeongsoo Nam** is Assistant Professor in Department of Smart City Architectural Engineering, College of Engineering at Chungnam National University, Daejeon, Republic of Korea.